J Muscle Res Cell Motil
DOI 10.1007/s10974-015-9412-6

ORIGINAL PAPER

High ionic strength depresses muscle contractility by decreasing both force per cross-bridge and the number of strongly attached cross-bridges

Li Wang[1,2] · Anzel Bahadir[3] · Masataka Kawai[2]

Received: 26 December 2014 / Accepted: 26 March 2015

Abstract An increase in ionic strength (IS) lowers Ca^{2+} activated tension in muscle fibres, however, its molecular mechanism is not well understood. In this study, we used single rabbit psoas fibres to perform sinusoidal analyses. During Ca^{2+} activation, the effects of ligands (ATP, Pi, and ADP) at IS ranging 150–300 mM were studied on three rate constants to characterize elementary steps of the cross-bridge cycle. The IS effects were studied because a change in IS modifies the inter- and intra-molecular interactions, hence they may shed light on the molecular mechanisms of force generation. Both the ATP binding affinity (K_1) and the ADP binding affinity (K_0) increased to 2–3x, and the Pi binding affinity (K_5) decreased to 1/2, when IS was raised from 150 to 300 mM. The effect on ATP/ADP can be explained by stereospecific and hydrophobic interaction, and the effect on Pi can be explained by the electrostatic interaction with myosin. The increase in IS increased cross-bridge detachment steps (k_2 and k_{-4}), indicating that electrostatic repulsion promotes these steps. However, IS did not affect attachment steps (k_{-2} and k_4). Consequently, the equilibrium constant of the detachment step (K_2) increased by ~100 %, and the force generation step (K_4) decreased by ~30 %. These effects together diminished the number of force-generating cross-bridges by 11 %. Force/cross-bridge (T_{56}) decreased by 26 %, which correlates well with a decrease in the Debye length that limits the ionic atmosphere where ionic interactions take place. We conclude that the major effect of IS is a decrease in force/cross-bridge, but a decrease in the number of force generating cross-bridge also takes place. The stiffness during rigor induction did not change with IS, demonstrating that in-series compliance is not much affected by IS.

Keywords Kinetics · Elementary steps · Debye length · Ionic atmosphere · Sinusoidal analysis · Rabbit psoas fibres

✉ Masataka Kawai
masataka-kawai@uiowa.edu

Li Wang
li-wang-1@suda.edu.cn

Anzel Bahadir
anzel78@hotmail.com

[1] School of Nursing, Soochow University, Suzhou 215006, Jiangsu, China

[2] Department of Anatomy and Cell Biology, Carver College of Medicine, University of Iowa, Iowa City, IA 52242, USA

[3] Department of Biophysics, Faculty of Medicine, Duzce University, Konuralp Campus, 81620 Duzce, Turkey

Introduction

The muscle produces force through myosin cross-bridges which cyclically attach to and detach from the thin filament. A myriad of factors within and outside of muscle cells can influence contraction and cause altered active tension production. It has been known that high ionic strength (IS) depresses contraction, leading to less active tension and stiffness production in skinned muscle fibres (Gordon et al. 1973; Kawai et al. 1990; Sugi et al. 2013). On the other hand, the unloaded shortening velocity is little affected by IS (Gulati and Podolsky 1978). Other studies suggest that the rate-limiting step for isometric tension production is different from that for isotonic shortening (Thames et al. 1974; Gulati and Podolsky 1981). However, the molecular mechanism of the IS effect is not well understood.

Published online: 03 April 2015

We know that IS in living muscle cells is controlled at around 215 mM (Godt and Maughan 1988), but studying at different ISs has a merit in that such studies can characterize the nature of the molecular interactions between macromolecules, because IS is one of the prominent factors to govern the inter- and intra-molecular interactions among myofibrillar proteins. The IS effect is also important, because many investigators in the past have used unphysiologically low IS solutions (such as 150 mM) to perform muscle fibre experiments (Wang et al. 2006; Kerrick et al. 2009; Borejdo et al. 2010; Mettikolla et al. 2011), hence it is essential to know how IS affects contractile properties to evaluate the significance of their findings.

In the current investigation, we aimed at studying the influence of IS on the cross-bridge kinetics, in particular, the effect of IS on the elementary steps of the cross-bridge cycle by using a small length perturbation analysis method, with the purpose of providing insights into the molecular mechanisms of contraction. Quite interestingly, we found that higher IS causes a decrease in the number of strongly attached cross-bridges, and at the same time, causes a decrease in force generated and/or supported by each cross-bridge. Rigor stiffness does not change much with IS, implying that the series compliance is not much affected by IS.

Materials and methods

Fibre preparations

New Zealand white rabbits of 3.5–5 kg weight was euthanized by injecting 150 mg/kg sodium pentobarbital into an ear vein. Strips of psoas muscles were excised. Small bundles (mostly 2 fibres/preparation, but some had 3 fibres, as identified under the dissecting microscope) of skinned psoas muscle were dissected and used in the present study. The fibre preparations were the same as described previously (Wang and Kawai 2013). The use of rabbits conformed with the current Guide for the Care and Use of Laboratory Animals (NIH publication DHSS/USPHS), and was approved by the University of Iowa's Animal Care and Use Committee.

Fibres ($\sim$75 μm in diameter and $\sim$3 mm in length) were mounted to the experimental apparatus with two ends fixed with a tiny amount of nail polish to two hooks made of stainless steel wire. One hook was connected to a length driver, and the other to a tension transducer. Relaxing solution was applied immediately and fibres were soaked in it for $\sim$10 min until the nail polish became dry and the connections were stable. The sarcomere length was adjusted to 2.5 μm by using He–Ne laser (wavelength: 0.6328 μm) diffraction pattern (first order was used), and then the fibre length and cross-sectional area were determined.

Solutions and experimental protocol

The experiments included the standard activation study, the MgATP study (referred to as ATP study for simplicity), the Pi study, the MgADP study (ADP study), and the rigor study. All experiments were performed at 20 °C. The solution compositions used for these studies are listed in Table 1. As indicated in this Table, adequate amounts of phosphocreatine (15 mM) and creatine kinase (80 units/ml) were added to all activating solutions, except for those used for the MgADP study. Acetate (Ac) was the major anion, because it preserves muscle fibers better than most other anions (Andrews et al. 1991). Na^+ concentration was minimized, because it comes in as Na_2H_2ATP and Na_2CP, and physiological Na^+ is at the low mM range (Godt and Maughan 1988). Consequently, the KAc concentration was adjusted to make different IS solutions.

An activating solution consisted of two parts: the first part was 66 mM CaEGTA, and the second part was the remainders (Labelled A in Fig. 1). pH of both parts were adjusted to 7.00 before mixing. The solution bathing the muscle preparation was washed twice with A (600 μl each) to ensure complete replacement. Tension did not develop, because adequate MgATP was present in the absence of Ca^{2+}. To activate the preparation, 60 μl of 66 mM CaEGTA was added, which are seen as a sudden rise of tension in Fig. 1. The content of the A solution was adjusted so that the final concentration of all components became the desirable concentration after mixing, and as shown in Table 1. In the standard activation study, four solutions containing 5 mM ATP, 8 mM Pi, and varied IS (150, 200, 250 or 300 mM) were applied to the fibres. The standard activating solution contained 8 mM Pi, because the resolution of process B is much better in this solution than the solution which does not contain Pi (Kawai 1986), and the rundown of the fibers is much less in this solution, primarily because of less active tension development. The better resolution of process B translates to the better resolution of step 4, because there are larger number of cross-bridges in the AM.ADP.Pi (AMDP in Scheme 1) and AM*ADP.Pi (AM*DP) states. The rigor solution was applied following the last activation (Fig. 1a, b). In order to avoid the systematic errors, different IS solutions were tested with increasing and decreasing orders alternatively in different fibres and the results were averaged.

The ATP, Pi and ADP studies are similar in their general procedures: fibres were tested with the standard activating solution (5 mM ATP, 8 mM Pi, and 200 mM IS) at the beginning and in the end of experiments, and rigor was induced following the last standard activation; solutions containing

Table 1 Solution compositions

	Pi study						ATP study			
	0P-150IS	20P-150IS	0P-200IS	0P-300IS	30P-200IS	30P-300IS	0S-150IS	0S-300IS	5S-150IS	5S-300IS
$K_2CaEGTA$	6	6	6	6	6	6	6	6	6	6
Na_2H_2ATP	5.96	5.92	6.11	6.41	6.05	6.35	–	–	5.94	6.39
Na_2CP	15	15	15	15	15	15	15	15	15	15
$HK_2PO_4 + H_2KPO_4$	–	20*	–	–	30*	30*	8*	8*	8*	8*
$MgAc_2$	6.51	6.35	6.68	7.02	6.44	6.78	1.52	2.04	6.44	6.95
NaAc	1.09	1.16	0.79	0.19	0.9	0.3	13	13	1.12	0.22
KAc	46.6	0.2	96.1	195	26.5	125.5	47.9	198.2	28	176.5
MOPS	10	10	10	10	10	10	10	10	10	10
KOH	16	21	16	16	24	24	6	55	18	18
CK (creatine kinase) (U/ml)	80	80	80	80	80	80	80	80	80	80

	ADP study						Relaxing	Rg-150IS	Rg-300IS
	00D-150IS	00D-300IS	0D-150IS	0D-300IS	3D-150IS	3D-300IS			
$K_2CaEGTA$	6	6	6	6	6	6		–	–
K_2H_2EGTA	–	–	–	–	–	–	6	–	–
Na_2H_2ATP	2.4	2.6	2.4	2.6	2.4	2.6	7	–	–
NaKADP	–	–	–	–	7.4	7.4	–	–	–
Na_2CP	15	15	–	–	–	–	–	–	–
$HK_2PO_4 + H_2KPO_4$	8*	8*	8*	8*	8*	8*	8*	8*	8*
$MgAc_2$	3.5	4.0	3.3	3.9	6.3	6.8	2	–	–
NaAc	8.2	7.9	38.2	37.8	27.1	26.7	41	55	55
KAc	39.9	189.5	54.5	204.1	34.7	184.2	71	72.1	222.8
MOPS	10	10	10	10	10	10	10	10	10
KOH	11	10	7	6	16	16	~19	6	5
A_2P_5	–	–	0.1	0.1	0.1	0.1	–	–	–

The total concentrations in mM are shown, except for CK which is shown in U/ml. * Equimolar mixture (the values are the total concentration). pH is adjusted to 7.00 ± 0.02 by KOH. pCa of the standard activating solution is 4.55

Ac Acetate, *CP* creatine phosphate, *Pi* phosphate, *S* ATP (0S and 5S: 0 and 5 mM ATP, respectively), *P* phosphate (0P, 20P, and 30P: 0, 20, and 30 mM phosphate, respectively), *Rg* rigor, A_2P_5 P1,P5-Di(adenosine-5′) pentaphosphate, trilithium salt

The 0.05–5 mM ATP solutions were created by appropriately mixing 0S and 5S solutions. Similarly, 0–20 mM Pi solutions (150 IS) or 0–30 mM Pi solutions (200–300 IS) were created by appropriately mixing 0P and 20P (or 30P) solutions. The standard activating solution is the same as the 5S solution in the ATP study, and the 8Pi solution in the Pi study. pCa of all activating solutions is ≤4.55, and $[Mg^{2+}]$ is 1 mM. $[Mg^{2+}] = 0.08$ mM for relaxing solution, and 0 mM for rigor solution

varied [ATP], [Pi] or [ADP] were applied between the two control activations. For the ATP study, the solutions containing differed ATP concentrations (0.05, 0.1, 0.2, 0.5, 1, 2, 5 mM ATP) at 150, 200, 250 and 300 mM IS were applied to fibres (all ATP concentrations at one IS was tested with the same preparation). For the Pi study, solutions containing differed Pi concentrations (0, 2, 4, 8, 14, and 20 mM Pi for 150 mM IS; and 0, 2, 4, 8, 16, and 30 mM Pi for 200, 250, and 300 mM IS) were applied to the fibres (all Pi concentrations at one IS was tested within the same preparation). Within the same IS, the 5 mM ATP solution in the ATP study, the 8 mM Pi solution in the Pi study, and the standard activation solution has the same compositions. Solutions of varied ADP concentrations (0, 1, 2, 3 mM ADP) were applied to fibres to study the effect of ADP with varied IS (150, 200, 250, and 300 mM). In rigor study, standard activating solution was first applied, which was followed by the rigor solution consisting of 150, 200, 250, and 300 mM IS (Fig. 1c). Because of the presence of multivalent ionic species and other essential ions needed for experiments (CP^{2-}, $CaEGTA^{2-}$, $Pi^{1.5-}$, $MgATP^{2-}$, ATP^{4-}, Mg^{2+}, MOPS) that increase IS, the lowest possible IS we have used was 150 mM. A home made computer program Multiple Equilibria (ME.exe) was used to calculate the solution recipes with the following apparent binding constants at pH 7.00 (log_{10} values are listed): CaEGTA 6.285, MgEGTA 1.613, CaATP 3.698,

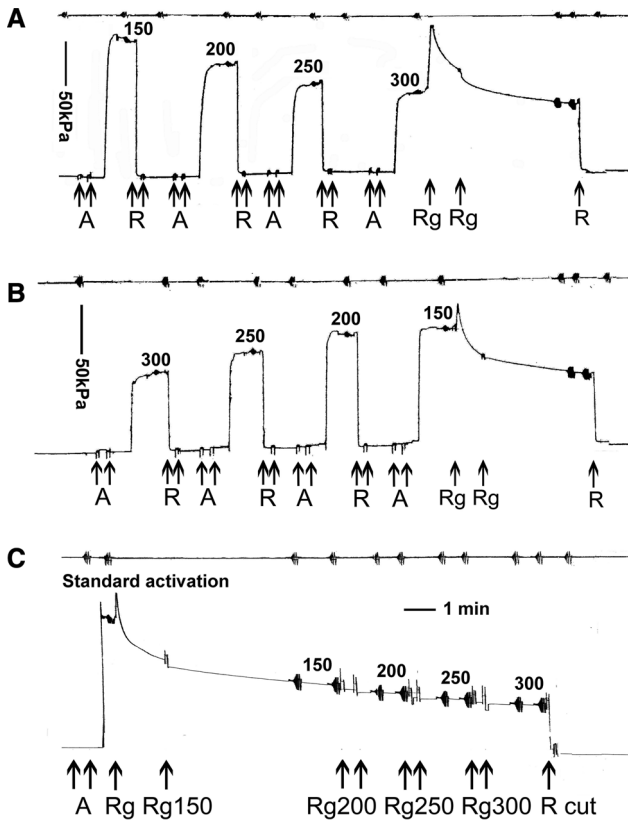

Fig. 1 Example of slow pen traces of standard activations and rigor induction. **a** A psoas muscle preparation was activated by standard solutions that contained 5 mM MgATP and 8 mM Pi of varying ionic strength (IS, indicated in mM) from 150 to 300 mM, followed by rigor induction with 200 mM IS rigor solution. **b** Another muscle preparation was activated by standard solutions at varying IS from 300 to 150 mM, followed by rigor induction with 200 mM IS rigor solution. **c** A third preparation was first activated by the standard solution with 200 mM IS, then rigor was induced with 150 mM IS solution, and IS was increased as indicated in mM. In the end, the fibres were cut to measure the blank coupling between length and force transducers. The peak-to-peak amplitude of the length change (*top trace in each panel*) was 0.25 % L_0. "*A*" is an activating solution without CaEGTA, which was changed twice to ensure complete solution change, and its IS varied depending on the experiment. Tension rises on addition of CaEGTA (final concentration: 6 mM, pCa 4.55). The IS value in mM is written in the figure where tension is at its peak. *Rg* indicates the rigor solution, and *R* indicates the relaxing solution; ionic strength of both solutions was 200 mM, and as define in Table 1. *Calibration bars* (tension and time) are the same for all panels

MgATP 4.004, K.ATP 0.792, NaATP 0.883, CaCP 1.148, MgCP 1.298, $CaAc_2$ 0.498, $MgAc_2$ 0.538, CaPi −3.665, MgPi −3.485, KPi −4.875, and NaPi −4.765.

Sinusoidal analysis

During tension plateau, sinusoidal analysis was performed to record tension transients. The sinusoidal analysis method has been previously described in detail (Kawai and Brandt 1980; Kawai 1982; Wang et al. 2013, 2014). During the standard activation, ATP, ADP, and Pi studies, the length of the fibres were oscillated in a sinusoidal wave form with 17 discrete frequencies (*f*): 0.25, 0.5, 1, 2, 3.1, 5, 7, 11, 17, 25, 35, 50, 70, 100, 130, 185, and 250 Hz; actual measurements were carried out from high to low frequencies, because the high frequency range has more interesting information than the low frequency range. Also, it takes longer time to collect the low frequency data compared to collect the high frequency data. The amplitude of the oscillations was kept at 0.125 %, which corresponds to ± 1.6 nm per half sarcomere and smaller than the cross-bridge's step size. If this is larger than the step size, the elementary steps of the cross-bridge cycle cannot be characterized.

The tension and length time course data were collected (see Fig. 2 of Kawai and Brandt 1980), and the complex modulus data $Y(f)$ were calculated as the ratio of tension change to length change at each frequency. $Y(f)$ is a frequency response function relating the length change (strain) to the tension change expressed in the frequency domain, and consists of two components: the viscous modulus (imaginary part of $Y(f)$) and the elastic modulus (real part of $Y(f)$). The complex modulus data were fitted to Eq. (1), which consists of three exponential processes A, B, and C, that are involved in active cross-bridge cycling (Eq. (2) in Kawai and Brandt 1980).

$$\underset{\text{Process A}}{} \quad \underset{\text{Process B}}{} \quad \underset{\text{Process C}}{}$$

$$Y(f) = H + \frac{Afi}{a + fi} - \frac{Bfi}{b + fi} + \frac{Cfi}{c + fi} \tag{1}$$

where $i = \sqrt{-1}$; a, b and c ($a < b < c$) are the characteristic frequencies of process A, B, and C; and $2\pi a$, $2\pi b$, and $2\pi c$ are the apparent rate constants of processes A, B and C, respectively. Process A is a low frequency-exponential advance (slow tension recovery), where the muscle absorbs net work from the length driver; process B is a medium frequency-exponential delay (delayed tension), where the muscle generates oscillatory work on the length driver; process C is a high frequency-exponential advance (fast tension recovery), where the muscle absorbs work (Kawai and Brandt 1980). A, B and C are their respective magnitudes (amplitudes). H is a constant that represents the elastic modulus at zero frequency. All of these processes are absent in the relaxed fibres, or in fibres in which rigor is induced (Kawai and Brandt 1980).

These seven parameters are uniquely determined from experimental results that consist of $17 \times 2 = 34$ points (viscous and elastic moduli for each frequency), hence the degree of freedom (N_{DF}) = 34–7 = 27. Because of this

Scheme 1 Elementary steps of the cross-bridge cycle in striated muscle fibres. The details can be found in Scheme 1 of (Wang et al. 2013)

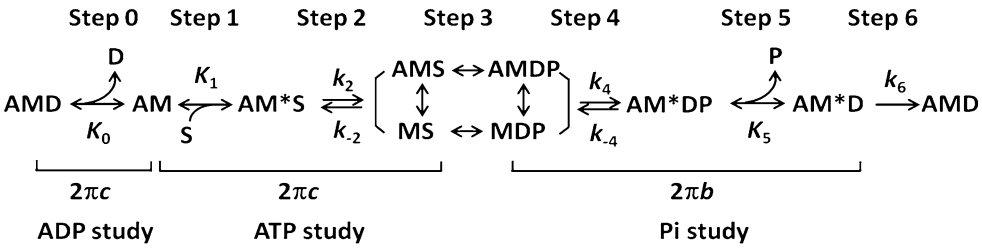

large N_{DF}, the 95 % confidence range for each frequency determination is about ± 19 % for 2π*a*, ± 12 % for 2π*b*, and ± 9 % for 2π*c* (Kawai and Brandt 1980). The elastic modulus extrapolated to the infinite (∞) frequency is defined as $Y_\infty = H + A - B + C$, where Y_∞ corresponds to phase 1 of step analysis; processes A, B, and C respectively corresponds to phases 4, 3, and 2 of step analysis (Heinl et al. 1974; Huxley 1974). Y_∞ is loosely called "stiffness" in muscle mechanics literature. The effects of ATP, ADP, and Pi on three exponential processes were used to characterize the elementary steps of the ATP binding, cross-bridge detachment, cross-bridge attachment (force generation), Pi release, and ADP release steps. Cross-bridge distribution at different states are calculated based on the kinetic constants of the elementary steps and Eqs. 8–14 of (Zhao and Kawai 1996). These data were also used to determine tension per cross-bridge as described (Kawai and Zhao 1993).

Statistical analysis

One-way ANOVA was used first to get the significance level, if $p < 0.05$, posthoc test was further applied for the comparison within each two groups. If Test of Homogeneity of Variance was proved ($p \geq 0.05$), Tukey posthoc test was chosen. Otherwise, Dunnett T3 posthoc test was used. All significance level was set at $p < 0.05$.

Results

Standard activation

The effect of IS on active tension and stiffness (Y_∞) was studied first with the standard activating solutions that contained 5 mM ATP and 8 mM Pi in the presence of creatine phosphate (CP) and creatine kinase (CK). As expected, we found that higher IS significantly depressed active tension and stiffness (Figs. 1a, b, 2a); the effect of IS on tension is consistent with previous reports (Gordon et al. 1973; Kawai et al. 1990; Sugi et al. 2013). The decrease amounted to 35 % in tension and 20 % in stiffness when comparing IS at 150 versus 300 mM. Therefore, the tension/stiffness ratio became smaller at higher IS (Fig. 2c). The values of tension, stiffness, and their ratio are listed in Table 2.

The complex modulus data $Y(f)$ gathered from standard activations are plotted as the viscous modulus versus frequency (Fig. 3a), the elastic modulus versus frequency (Fig. 3b), and the viscous modulus versus elastic modulus (Nyquist plots) (Fig. 3c) at four different IS. Each Nyquist plot (Fig. 3c) shows three contiguous semicircles, hence the complex modulus can be resolved into three exponential processes (A, B, and C) as shown in Eq. 1. The data were fitted to Eq. 1 and the best-fit curves are entered in Fig. 3 by continuous lines. The viscous modulus was affected by IS most significantly at around process C (the rightmost peak in Fig. 3a), but the elastic modulus was affected by IS in all frequency ranges (Fig. 3b). In Nyquist plots, the semi-circles b and c were smaller at higher IS (Fig. 3c) demonstrating that the exponential processes B and C were diminished as isometric tension was decreased.

The apparent rate constants 2π*a*, 2π*b*, and 2π*c*, and their magnitudes (*A*, *B*, and *C*) were extracted from the complex modulus data and plotted in Fig. 4a, b. The apparent rate constants showed different responses to the IS change (Fig. 4a). 2π*a* is the slowest rate constant, centered around ∼5 s^{-1}, and did not change significantly from 150 to 300 mM IS. 2π*b* (centered ∼135 s^{-1}) and 2π*c* (centered ∼200 s^{-1}) increased with an increase in IS from 150 to 250 mM, and saturated at IS 250–300 mM. Magnitude *A* was about 3 MPa, and it did not change significantly with the IS change. Magnitudes *B* and *C* were 4–6 times of magnitude *A*, and they did not change much between IS 150 and 200 mM, but decreased at IS 200–300 mM (Fig. 4b). Magnitudes *B* and *C* changed similarly with the change in IS (Fig. 4b). Quite interestingly, when *C* was plotted against *B* for different fibres and different IS, they fell on the same line that extrapolated to the origin (Fig. 4c), demonstrating that *B* and *C* are proportionately related. Magnitude *H* is the stiffness extrapolated to zero frequency, it has a small value in fast twitch skeletal muscle fibres, and decreased with IS (Table 2).

ATP study

Both tension and stiffness generally decreased towards higher [ATP] at IS = 300, 250 mM, and possibly at 200 mM, but they did not change much at 150 mM (Fig. 5a, b; the [ATP] is shown in the log scale). The decrease was

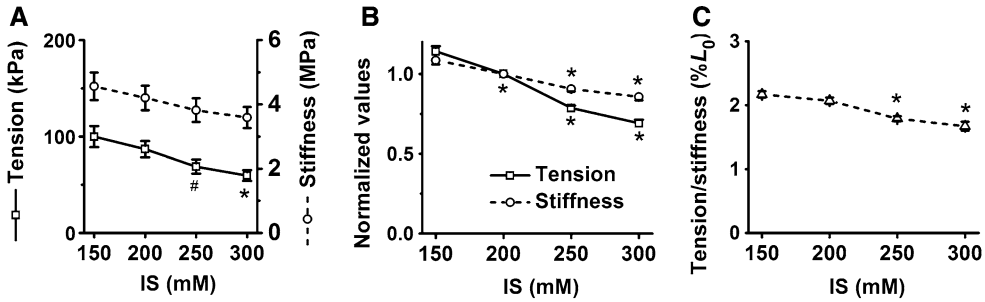

Fig. 2 Parameters obtained from the standard activations are plotted as functions of IS. **a** Tension and stiffness, **b** tension and stiffness normalized to their respective values at 200 mM IS, and **c** the tension/stiffness ratio. *Error bars* represent the standard errors of the mean (SEM), many of which are smaller than the symbol size and cannot be seen. n = 10 for each IS. $^{*}P < 0.05$ compared to the respective parameter at 150IS (*at 200 mM is for tension, and not for stiffness). $^{\#}P = 0.056$ compared to tension at 150IS

Table 2 Values of tension and stiffness in the standard activating solution (ATP = 5 mM, Pi = 8 mM)

	150 IS	200 IS	250 IS	300 IS	Units
Tension	100 ± 11	87 ± 8	69 ± 7*	60 ± 6*	kPa
Tension	1.142 ± 0.032	1	0.786 ± 0.016*	0.691 ± 0.022*	Normalized
Stiffness	4.6 ± 0.4	4.2 ± 0.4	3.8 ± 0.4	3.6 ± 0.3	MPa
Tension/Stiffness	2.17 ± 0.05	2.07 ± 0.05	1.79 ± 0.04*	1.67 ± 0.07*	%L_0
Force/CB (T_{56})	1.10 ± 0.07 (10)	1.00 ± 0.02 (11)	0.95 ± 0.03 (12)	0.81 ± 0.03 (11)*	Normalized
App rate const 2πa	4.80 ± 0.31	4.77 ± 0.16	4.70 ± 0.21	4.98 ± 0.27	s^{-1}
App rate const 2πb	132 ± 3	144 ± 2*	153 ± 2*	146 ± 6*	s^{-1}
App rate const 2πc	191 ± 5	200 ± 3	222 ± 3*	235 ± 10*	s^{-1}
Magnitude A	2.93 ± 0.29	2.87 ± 0.28	2.88 ± 0.31	2.82 ± 0.28	MPa
Magnitude B	15.6 ± 2.0	15.1 ± 1.6	13.5 ± 1.8	11.3 ± 1.7	MPa
Magnitude C	16.5 ± 2.1	15.8 ± 1.6	13.8 ± 1.8	11.6 ± 1.7	MPa
Magnitude H	0.79 ± 0.08	0.71 ± 0.08	0.58 ± 0.06	0.48 ± 0.06*	MPa

n = 10 for all experiments, except for those specified in (). The tension values are small, because of the presence of 8 mM Pi. For normalized tension, the data on each preparation were first normalized to the value at 200 mM IS, and then averaged. T_{56} (force/cross-bridge) was deduced by fitting tension versus [Pi] data to Eq. 4, and it represents force supported by cross-bridges (CB) in the states AM*DP and AM*D (major force-generating cross-bridges), and normalized to the value at 200 mM IS

* $P < 0.05$ when compared to the corresponding value at 150 IS

larger in higher IS, indicating that larger IS increases the sensitivity of tension and stiffness to ATP. The tension/stiffness ratio were similar at different [ATP] within each IS; the ratio was smaller in higher IS (Fig. 5c), which is consistent with the result in the standard activation (Fig. 2c).

The apparent rate constant 2πa generally increased at low [ATP] (0.05–0.5 mM) and saturated at high [ATP] (0.5–5 mM). The increase was more prominent at 150–200 mM IS (Fig. 6a). At 250–300 mM IS, there was an extra maximum at 0.1–0.2 mM ATP. The rate constant 2πb showed a monotonic increase with an increase of ATP in all IS solutions similarly (Fig. 6b). The increase was almost linear in the semi log plots. The rate constant 2πc showed an increase from 0.05 to 5 mM ATP. 2πc at 0.05 mM ATP was not much different among different IS solutions, indicating that the rate constant k_{-2} of the reverse detachment step does not change much with IS. At 5 mM ATP 2πc was significantly larger at higher IS (Fig. 6c), indicating that the rate constant k_2 of the detachment step increases with IS. Magnitude parameters A, B, and C became larger and approached saturation when [ATP] was increased from 0.05 to 5 mM (Fig. 6d–f). The concentration of their mid (½) points decreased as IS was raised, indicating that their sensitivity to ATP was increased with IS. Their differences were bigger in B and C than in A.

The data of 2πc versus [ATP] (Fig. 6c) were fitted to Eq. 2 (Kawai and Halvorson 1989) to deduce the ATP association constant (K_1), and the rate constants (k_2, k_{-2}) of the cross-bridge detachment step (Scheme 1).

$$2\pi c = \frac{K_1 S}{1 + K_0(D + D_0) + K_1 S} k_2 + k_{-2} \quad (2)$$

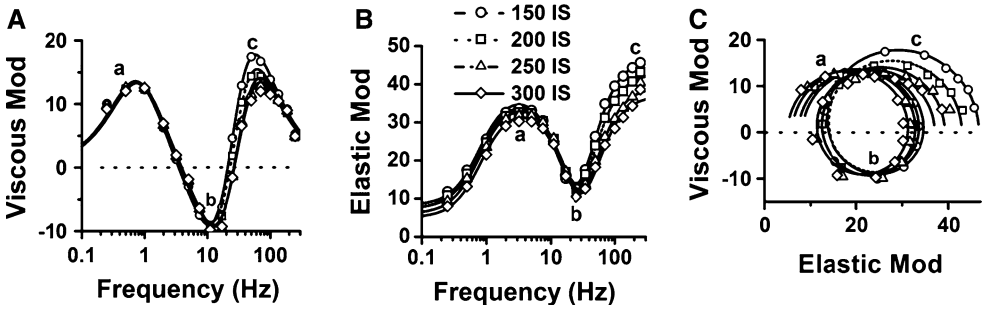

Fig. 3 The complex modulus data $Y(f)$ averaged for the standard activations at four IS. The data are plotted as **a** viscous modulus [=*Imag* $Y(f)$] versus frequency, **b** elastic modulus [=*Real* $Y(f)$] versus frequency, and **c** viscous modulus versus elastic modulus (Nyquist plot). *Symbols* are the same for all panels and represent the average of 10 experiments. The *continuous curves* represent the best-fit curves to Eq. 1. The units of moduli are MPa

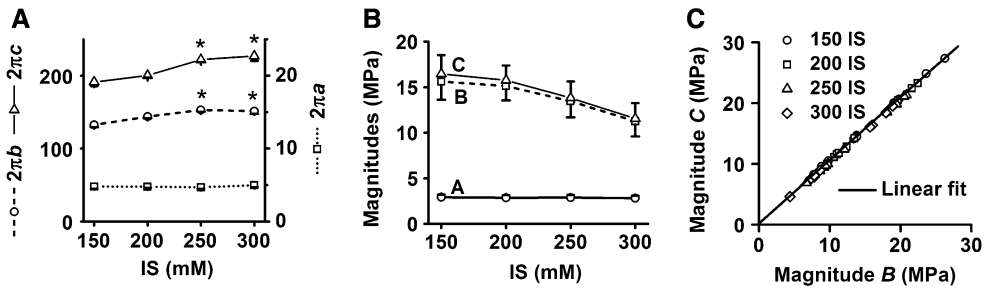

Fig. 4 Parameters of exponential processes deduced from standard activations are plotted as functions of IS. **a** The apparent rate constants (unit: s^{-1}), **b** their magnitudes, and **c** correlation between magnitudes B and C. The *regression line* corresponds to $C = 1.037B + 0.025$ MPa with $R^2 = 0.999$. These parameters are deduced by fitting the complex modulus data to Eq. 1. In **a** and **b**, *error bars* represent SEM; in **a** they are mostly smaller than the symbol size. n = 10 for each IS. $^*P < 0.05$ compared to the respective parameter at 150IS

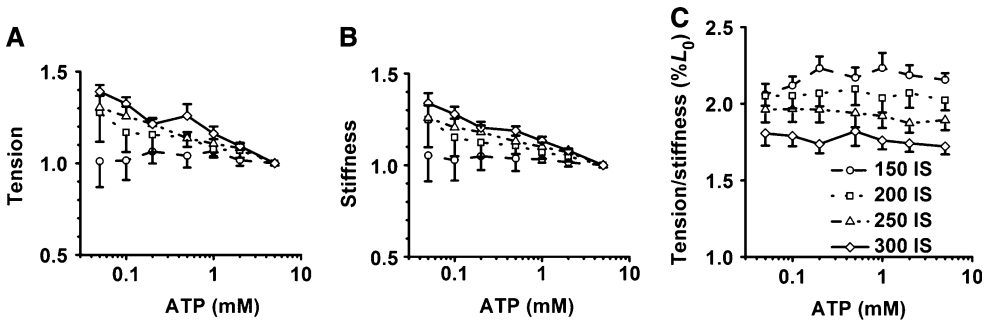

Fig. 5 Tension and stiffness deduced from the ATP study are plotted at four IS. The data are plotted as **a** tension versus [ATP], **b** stiffness versus [ATP], and **c** tension/stiffness versus [ATP]. Tension and stiffness are normalized to their respective values at 5 mM ATP, which can be found in Fig. 2a. The number of fiber preparations (n) are 7, 9, 11, and 11 for 150, 200, 250, and 300 mM IS, respectively. *Symbols* for each IS are the same for all panels

where S = [MgATP], D = [MgADP], D_0 = contaminating [MgADP]. For the ATP study, the $D + D_0$ term was set to 0. The results of the fitting are entered in Fig. 6c as continuous curves, and the fitted parameters are plotted in Fig. 7. K_1 increased with an increase in IS from 150 to 250 mM, and no further increase was observed at 250–300 mM (Fig. 7a). The rate constant of detachment step (k_2) increased significantly with the increase in IS, but that of its reversal step (k_{-2}) did not change much (Fig. 7b). These resulted in a significant increase in the equilibrium constant of the cross-bridge detachment step ($K_2 = k_2/k_{-2}$) with the increase in IS (Fig. 7a).

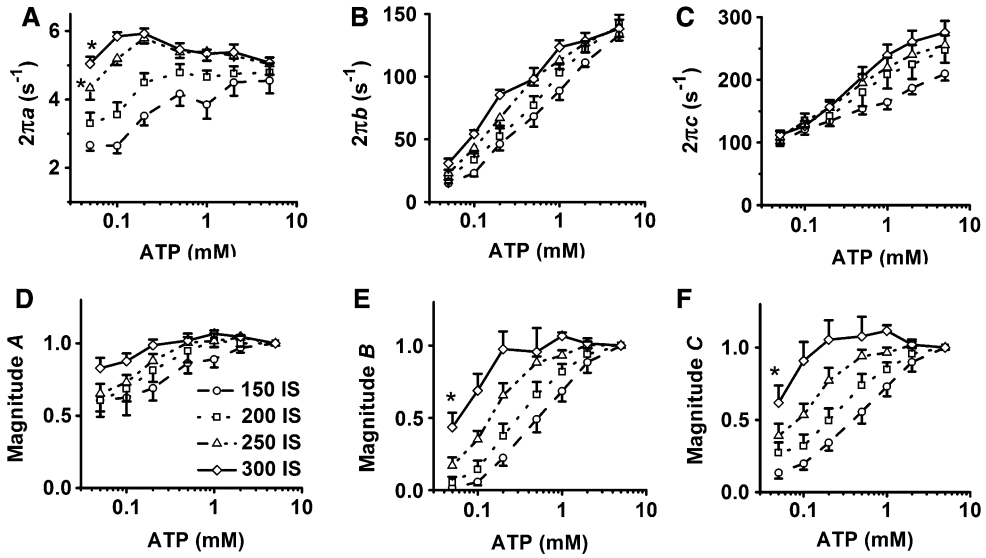

Fig. 6 Parameters of exponential processes deduced from the ATP study at four different IS. The data are plotted as **a** apparent rate constant $2\pi a$ versus [ATP], **b** $2\pi b$ versus [ATP], **c** $2\pi c$ versus [ATP], **d** magnitude A versus [ATP], **e** B versus [ATP], and **f** C versus [ATP]. In **c** *continuous curves* represent the best fit curves to Eq. 2. In (**d**–**f**), the data were normalized to their respective values at 5 mM ATP; their absolute values can be found in Fig. 4b. n = 7, 9, 11, and 11 for 150, 200, 250, and 300 mM IS, respectively. *Symbols* for each IS are the same for all panels. $^*P < 0.05$ compared to the respective parameter at 150IS

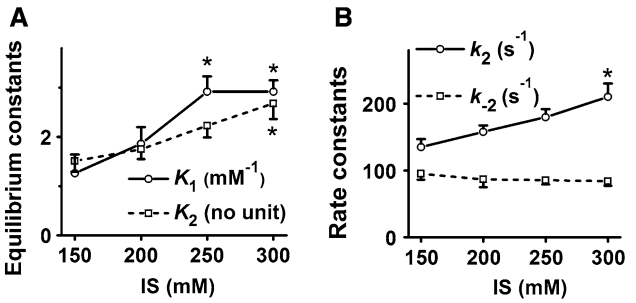

Fig. 7 The kinetic constants of elementary steps deduced from the ATP study are plotted as functions of IS. **a** The ATP association constant (K_1, *open circle*), and the equilibrium constant of the cross-bridge detachment step (K_2, *open square*). **b** The forward (k_2, *open circle*) and reversal (k_{-2}, *open square*) rate constants of the cross-bridge detachment step. The number of fiber preparations (n) are 7, 8, 11, and 11 for 150, 200, 250, and 300 mM ionic strength, respectively. $^*P < 0.05$ compared to the respective parameter at 150IS

Pi study

The effect of [Pi] was studied between 0 and 30 mM. Both tension and stiffness decreased with an increase in [Pi], and the effects were more significant at higher IS (Fig. 8). With an increase in [Pi], the tension decrease was larger than stiffness decrease (Fig. 8a, b), resulting in a decrease in the tension to stiffness ratio (Fig. 8c). The ratio at 150 and 200 mM IS was larger than that at 250 and 300 mM IS at a given [Pi] (Fig. 8c). With sinusoidal analysis, the apparent rate constant $2\pi a$ did not change much with [Pi], except for a small effect at 0–2 mM Pi at 150 mM IS (Fig. 9a). $2\pi b$ increased significantly at low mM concentration of Pi, and approached saturation when [Pi] was increased to 30 mM (Fig. 9b); the increase was less in 150 mM IS solution than that in 200–300 mM IS solutions. In 200–300 mM IS solutions, $2\pi c$ decreased first from 0 to 4 mM Pi, and then increased somewhat at higher [Pi] (Fig. 9c). In 150 mM IS solutions, the initial decrease was not evident, but the increase at higher [Pi] was evident. The initial decrease in $2\pi c$ indicates that Pi competitively inhibits the ATP binding to the nucleotide binding pocket (Candau and Kawai 2011), which is more enhanced at higher IS (Fig. 9c).

Magnitude A did not change significantly when [Pi] was increased in all IS solutions tested, but there was some IS effects (Fig. 9d). Magnitudes B and C increased significantly at low [Pi] and saturated at high [Pi], and these effects were similar in all IS solutions studied (Fig. 9e, f).

The data of $2\pi b$ versus [Pi] were fitted to Eq. 3 (Kawai and Halvorson 1991) (Fig. 9b, continuous curves) to deduce the rate constants (k_4, k_{-4}) of the force generating (cross-bridge attachment) step and the Pi association constant (K_5) as functions of IS.

$$2\pi b = \sigma k_4 + \frac{K_5 P}{1 + K_5 P} k_{-4} \tag{3}$$

where P = [Pi], and $\sigma = \frac{K_2 K_1 S}{1+(1+K_2)K_1 S}$.

The results are plotted in Fig. 10. k_4 did not change much with IS, but that of its reversal step (k_{-4}) increased significantly with IS (Fig. 10b). This resulted in a decrease of the equilibrium constant of this step ($K_4 = k_4/k_{-4}$) with

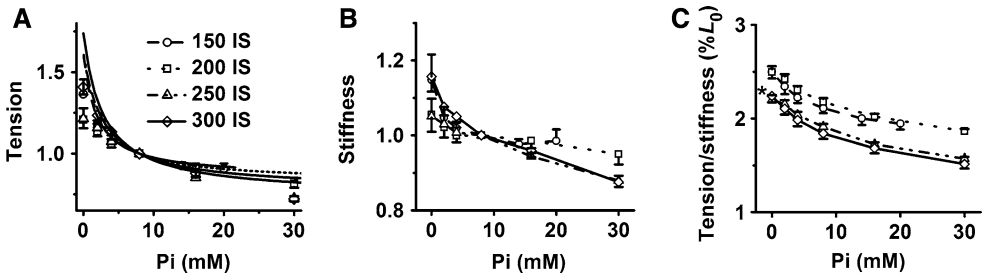

Fig. 8 Tension and stiffness deduced from the Pi study are plotted at four IS. **a** Tension versus [Pi], in which *continuous curves* represent the best fit curves to Eq. 4, **b** stiffness versus [Pi], and **c** tension/stiffness versus [Pi] plots. Tension and stiffness are normalized to their respective values at 8 mM Pi; their absolute values can be found in Fig. 2a. n = 10, 11, 12, and 11 for 150, 200, 250, and 300 mM IS, respectively. *Symbols* for each IS are the same for all panels. *$P < 0.05$ for both 250IS and 300IS versus the one at 150IS

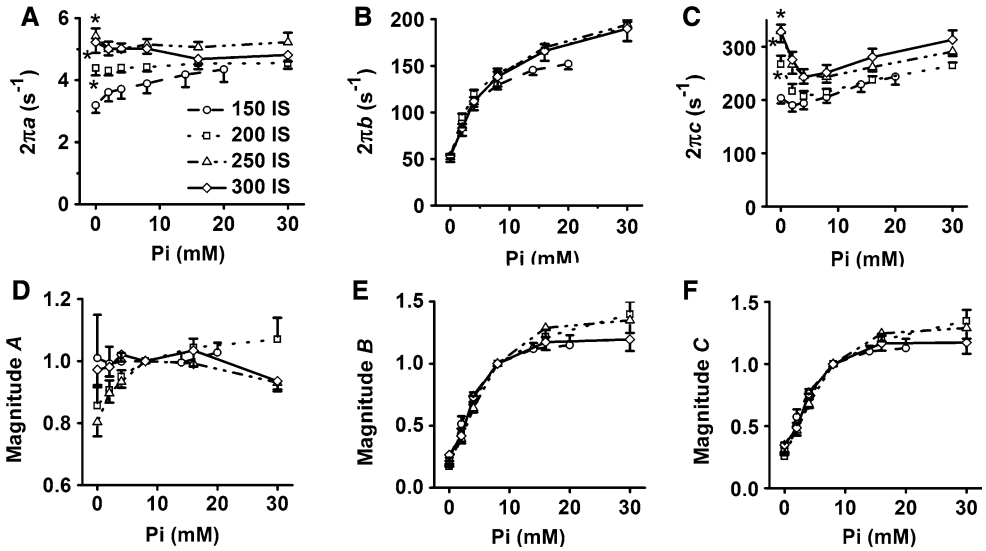

Fig. 9 Parameters of exponential processes deduced from the Pi study at four IS. The data are plotted as **a** the apparent rate constant $2\pi a$ versus [Pi], **b** $2\pi b$ versus [Pi], in which *continuous curves* represent the best fit curves to Eq. 3, **c** $2\pi c$ versus [Pi], **d** magnitude *A* versus [Pi], **e** magnitude *B* versus [Pi], and **f** magnitude *C* versus [Pi]. In **b** *continuous curves* represent best fit curves to Eq. 3. In **d**–**f**) the data were normalized to their respective values at 8 mM Pi; their absolute values can be found in Fig. 4b. n = 10, 11, 12, and 11 for 150, 200, 250, and 300 mM IS respectively. *Symbols* for each IS are the same for all panels. *$P < 0.05$ compared to the respective value at 150IS. *Asterisk* is entered only for the 0 mM Pi condition

an increase in IS from 150 mM to 250 mM (Fig. 10a), but no further decrease was observed at 300 mM IS. Similarly, K_5 decreased when IS was increased from 150 to 250 mM, but no further decrease was observed at 300 mM (Fig. 10a).

The tension versus [Pi] data (Fig. 8a) were fitted to Eq. 4 (Kawai and Zhao 1993).

$$Tension = T_0X_0 + T_1X_1 + T_2X_2 + T_5X_5 + T_6X_6 = \quad (4)$$

where X_0, X_1, X_2, X_4, and X_5 are probability of cross-bridges at states AMD, AM, AMS, AM*DP, AM*D, respectively; T_0, T_1, T_2, T_5, and T_6 are tensions supported by the respective states; $\varepsilon = T_1/T_6 = 0.79$ and $\zeta = T_2/T_6 = 0.48$ are empirically derived parameters, $X_0 \approx 0$ in the presence of CP/CK, and $T_{56} = T_5 = T_6$ in rabbit psoas fibres (Kawai and Zhao 1993). T_{56} (tension per cross-bridge) is the tension supported by cross-bridges at states AM*DP and AM*D. In order to avoid the scatter of the data owing to the uncertainty of the estimate of the cross-sectional area, the T_{56} data were normalized against that of 200 mM IS (181 ± 15 kPa, n = 11), and results are plotted in Fig. 10c. T_{56} decreased by about 9, 14, and 26 % when IS was increased from 150 mM to 200, to 250, and to 300 mM, respectively, demonstrating smaller changes compared to the overall tension of fibres (decreased by 13, 31, and 40 % respectively) (Fig. 2a; Table 2). Therefore, the decrease of tension in fibres was larger than the decrease of tension per cross-bridge.

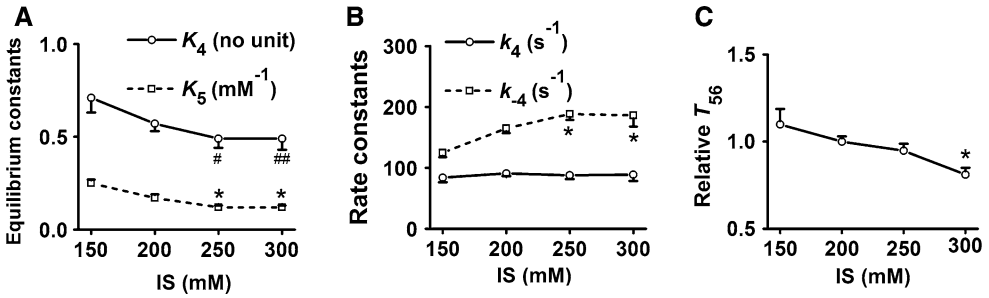

Fig. 10 The kinetic constants of the elementary steps deduced from the Pi study are plotted as functions of IS. **a** The equilibrium constant of the force generation step (K_4, *open circle*), and the Pi association constant (K_5, *open square*). **b** The forward (k_4, *open circle*) and reversal (k_{-4}, *open square*) rate constants of the force generation step. **c** Tension per cross-bridge (T_{56}), normalized to the tension of the first standard activation with 200 mM IS (181 ± 15 kPa). n = 10, 11, 12, and 11 for 150, 200, 250, and 300 mM IS respectively. $^{*}P < 0.05$ compared to the respective parameter at 150IS. $^{\#}P = 0.059$ and $^{\#\#}P = 0.075$ compared to the respective value at 150IS

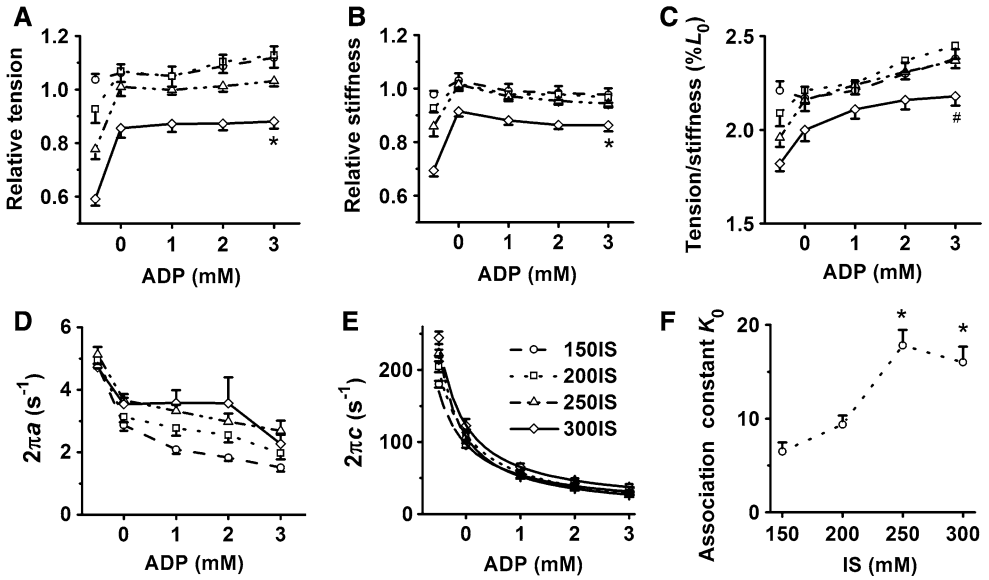

Fig. 11 Parameters deduced from the ADP study at four IS. The data are plotted as **a** tension versus [ADP], normalized to that of the standard activation with 200 mM IS, **b** stiffness versus [Pi], normalized similarly, **c** tension/stiffness versus [ADP], **d** apparent rate constant $2\pi a$ versus [ADP], **e** apparent rate constant $2\pi c$ versus [ADP], and **f** K_0 (ADP association constant) versus IS. In **e** *continuous curves* represent best fit curves to Eq. 2; At 0 mM ADP, solutions with/without CP/CK were used to extrapolate the data and to obtain D_0, the excess (contaminating) [ADP] in the 0 mM ADP solution. D_0 generally resulted in the range 0.48–0.75 mM. n = 10 for each IS. *Symbols* for each IS are the same for panels (**a**–**e**). $^{*}P < 0.05$ compared to the respective value at 150IS. $^{\#}P = 0.051$ compared to the respective value at 150IS

ADP study

The effect of [ADP] in four different IS solutions was studied by applying ADP series solutions (00*D*, 0*D*, 1*D*, 2*D*, and 3*D*, where *D* = [ADP] in mM) of 150, 200, 250, and 300 mM IS to fibres. 0*D*–3*D* solutions contained 2 mM ATP, 8 mM Pi, and 100 μM A_2P_5 (P1,P5-Di(adenosine-5′) pentaphosphate, trilithium salt: adenylate kinase inhibitor). The 00*D* solution, which contained CP and CK but no A_2P_5 or ADP, was tested first (leftmost points in Fig. 11a–e). This was followed by the 0–3*D* solutions in the increasing order. These solutions contained specified (added) concentrations of ADP (0–3 mM) and A_2P_5, but no CP/CK. The purpose was to detect the ADP binding constant (K_0), and the extra [ADP] (D_0) in the 0D-3D solutions by extrapolation (Fig. 11e); D_0 is a finite positive number ($D_0 > 0$) because of ADP contamination in ATP, and continuous hydrolysis of ATP in fibres.

Tension (Fig. 11a) and stiffness (Fig. 11b) increased when the solution was changed from 00*D* to 0*D*, and remained at about the same level from 0*D* to 3*D*. As expected, they were smaller at higher IS at each [ADP] (Fig. 11a, b). The apparent rate constant $2\pi a$ became smaller at larger [ADP] (Fig. 11d). At 00D, $2\pi a$ was similar among all IS, and the IS difference became evident

at higher IS in the 0*D*–3*D* solutions (Fig. 11d). At 00*D*, the apparent rate constant $2\pi c$ was larger at higher IS, but this difference converged in the 0*D*-3*D* solutions (Fig. 11e). Process B was prominent with 00*D*, diminished in 0*D*, and absent in 1-3*D* solutions. Fitting the $2\pi c$ data versus [ADP] (Fig. 11e, continuous curves) to Eq. 2 allowed us to determine K_0 (ADP association constant) and D_0. K_0 significantly increased from 150 to 250 mM IS, and remained at the same level in 300 mM IS (Fig. 11f). This effect is similar to that of ATP (Fig. 7a). D_0 was 0.75 ± 0.19 mM (n = 10) in 150 mM IS, 0.51 ± 0.09 mM (n = 10) in 200 mM IS, 0.48 ± 0.04 mM (n = 10) in 250 mM IS, and 0.52 ± 0.07 mM (n = 10) in 300 mM IS. These values are not significantly different among different IS, and the overall average was 0.57 ± 0.06 mM (n = 40).

Cross-bridge distribution

A mixture of the detached states, weakly attached states, and strongly attached states exists during active cross-bridge cycling. Based on the kinetic constants deduced from the ATP, Pi, and ADP studies, the cross-bridges distribution among different states were calculated by using Eqs. 7–12 of (Zhao and Kawai 1994) with $S = 5$ mM, $P = 8$ mM, and $D = 0.02$ mM. The results are plotted in Fig. 12, where *Att* indicates the strongly attached states:

$$Att = [\mathrm{AM} * \mathrm{D}] + [\mathrm{AM} * \mathrm{DP}] + [\mathrm{AM} * \mathrm{S}] + [\mathrm{AM}] + [\mathrm{AMD}] = X_6 + X_5 + X_2 + X_1 + X_0.$$

Det indicates the summation of truly detached states and weakly attached states: $Det = [\mathrm{MDP}] + [\mathrm{MS}] + [\mathrm{AMDP}] + [\mathrm{AMS}] = X_{34} = 1 - Att$, and shown in […] in Scheme 1. We found that, when IS was increased, the number of strongly attached cross-bridges decreased. Compared to the value at 150 mM IS, the decrease amounted to ~7 % at 200–250 mM IS, and ~10 % at 300 mM) (Fig. 12, Att). This partly explains the less tension and stiffness at higher IS (Fig. 2a).

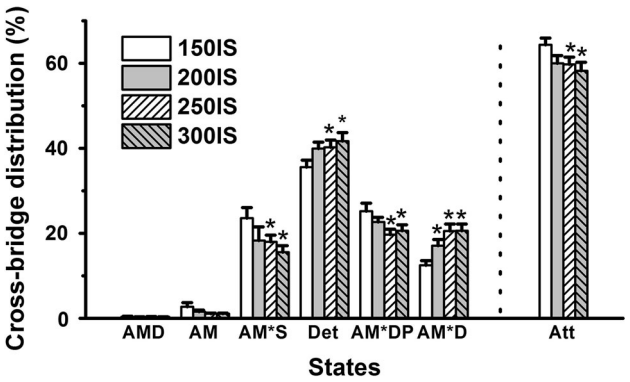

Fig. 12 Cross-bridge distributions among six states at the standard activating conditions ($S = 5$ mM, $P = 8$ mM, $D = 0.02$ mM). *Det* Detached state, including all detached states (MS, MDP) and weakly attached states (AMS, AMDP); these are shown in [] in Scheme 1. *Att* The sum of strongly attached states (AMD, AM, AM*S, AM*DP, and AM*D). Because *D* is small, the distributions at the AMD state are in the range 0.17–0.24 %, and not readily visible. *$P < 0.05$ compared to the respective value at 150IS

Rigor tension and stiffness

To determine if the series compliance change with IS, rigor was induced from the standard activation at 200 mM IS, and rigor solutions of varying IS were applied (Fig. 1c). As seen in this figure, rigor tension was initially larger than active tension, but it gradually declined with time. This decline is always observed with rigor tension, and it is due to a gradual slipping (detachment and reattachment) of cross-bridges to a lesser force position, thereby registering less amount tension, as observed during in vitro motility assays when external force was applied to cross-bridges (Kawai et al. 2006). Rigor stiffness was measured at 100 Hz. Rigor tension and stiffness were normalized to their respective values at 200 mM IS, and the results are plotted in Fig. 13. As shown in this figure, there was no significant difference in tension or stiffness among different IS, indicating that the series compliance does not change its elastic property much when IS was changed between 150 and 300 mM.

Tension reproducibility and possible extraction of the thick filament

It has been known for some time that high IS, such as 730 mM, extracts the thick filament from sarcomeres, because the ionic interaction between neighboring light meromyosins (LMM) gives the stability to the thick filament backbone, and high IS weakens this interaction (Hanson and Huxley 1957). Although the highest IS we have used is 300 mM and far from 730 mM, one may

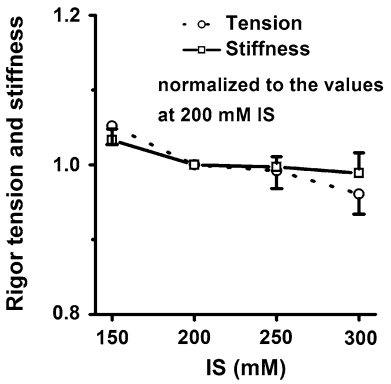

Fig. 13 Rigor tension and stiffness are plotted as functions of IS. The data were normalized to their respective values at 200 mM IS. n = 13 for each IS. Note that the origin is not included in the ordinate

suspect that there might be a partial extraction of the thick filament. To answer this question directly, we measured the control active tension at 200 mM IS before and after measurements were performed at 300 mM IS. Between the control activations, there were 14 intervening activations, each lasted for 40 s. Our results show that the ratio of isometric tension of the last control activation to the fast control activation was 95 ± 2 % (N = 11). This high reproducibility indicates that there was no significant extraction of the thick filament under our experimental conditions.

Discussion

General observations

In this investigation, we examined the contractility and cross-bridge kinetics in skinned rabbit psoas fibres in solutions containing different IS in the range of 150–300 mM, and varying concentrations of ligands (ATP, Pi, and ADP). Our aim was to determine whether force/cross-bridge or the number of force-generating cross-bridges changes with IS. Firstly, our results show that the increase in IS depresses maximal isometric tension and stiffness (Fig. 3a) as found previously (Gordon et al. 1973; Kawai et al. 1990; Yan et al. 1996; Sugi et al. 2013), and the depression is larger in tension than in stiffness (Fig. 2b) (Seow and Ford 1993; Iwamoto 2000). Secondly, our study demonstrates that IS affects the exponential processes measured in the complex moduli (Fig. 3) originated from tension transients. Elevated IS increases the sensitivity of the rate constant $2\pi c$ to the ligands (Figs. 6c, 9c, 11e). The magnitude parameters B and C decrease with IS, but magnitude A does not (Fig. 4b). Thirdly, IS affects the elementary steps of the cross-bridge cycle by increasing the association constants of the ATP and ADP binding steps (larger K_1 and K_0) and subsequent cross-bridge detachment step (K_2) (Fig. 7a), and by decreasing the equilibrium constant of force generation step (K_4) and the association constant of the Pi binding step (K_5) (Fig. 10a). These changes results in a decrease in the number of strongly attached cross-bridges that generate force (Fig. 12, Att). Increased IS also results in decreased force per cross-bridge (T_{56}) (Fig. 10c). In contrast, a change in IS does not significantly affect rigor tension and stiffness (Fig. 13).

The mechanism underlying the IS effects

Isometric tension on Ca^{2+} activation is generated through the strong and stereospecific attachment of myosin cross-bridges to the thin filament, and it decreases with an increase in IS (Fig. 2a). This decrease may be due to a decreased number of force-generating cross-bridges, to decreased force that each cross-bridge generates, and/or to the reduction of the stiffness of in-series elements.

Why does the IS affect cross-bridge kinetics?

The change in IS affects the ionic atmosphere in which charged molecules interact by the electrostatic force, and higher IS weakens this force by shrinking the ionic atmosphere. The atmosphere extends approximately to Debye length (l_D), which is reciprocally proportional to the square root of IS (Eq. 5). The Debye length is calculated in Fig. 14 (solid curve) based on Eq. 9.44 of Moore (1962), and it is 29 % less at 300 mM IS compared to that at 150 mM IS. Also plotted in Fig. 14 is force/cross-bridge (T_{56}) with proper scaling; the data were taken from Fig. 10c. As seen in this figure, force/cross-bridge closely correlates with the Debye length as IS is changed. Our purpose was to find out how IS affects the elementary steps of the cross-bridge cycle.

We found an increase in IS accelerated the apparent rate constants $2\pi b$ and $2\pi c$ (Fig. 4a). This is caused by increases in K_1 and k_2 (Fig. 7), because both $2\pi b$ and $2\pi c$ are positively correlated with K_1 and k_2 (Eq. 2 and Kawai and Halvorson 1991). The increase in k_2 and no change in k_{-2} (Fig. 7b) results in the increase of K_2 ($=k_2/k_{-2}$, Fig. 7). Similarly, the accelerated apparent rate constant $2\pi b$ with the IS increase (Fig. 4a) is caused by an increase in k_{-4}, because $2\pi b$ is positively and linearly correlated with k_{-4} (Eq. 3) (Kawai and Halvorson 1991). The significantly increased k_{-4} with little change in k_4 (Fig. 10b) causes the

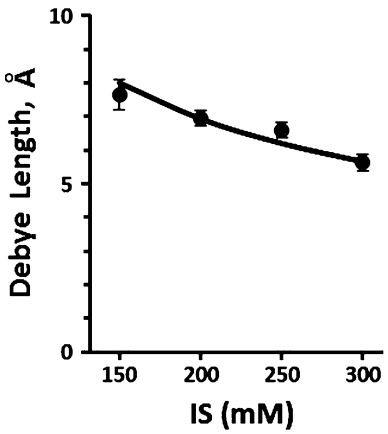

Fig. 14 The Debye length (l_D) (*curved* line) calculated from Eq. 5 that was derived from Eq. 9.44 of Moore (1962): $l_D = \sqrt{\frac{qkT}{(IS)}}$ (5) where k = 1.3805 x 10^{-23} JK^{-1} (Boltzmann constant), T = absolute temperature, and q = 23.36 $m^2J^{-1}M$. Force/cross-bridge (T_{56}, Fig. 10c) is replotted here (•) with proper scaling. At 20°C, l_D = 6.9 Å, 13.8 Å, and 30.7 Å for IS = 200 mM, 50 mM, and 10 mM, respectively

smaller K_4 at increased IS. In another words, the reverse rate of force generation is sensitive to the IS change, but the forward rate is not. Consequently, the high IS depresses isometric tension in active muscle fibres mainly through affecting the cross-bridge detachment rates represented by k_2 and k_{-4}, instead of the attachment rates represented by k_{-2} and k_4. This conclusion is generally consistent to that of (Seow and Ford 1993).

Because an increase in IS shields the electrostatic interaction (Maughan and Godt 1980), one may expect that, if the cross-bridge attachment is promoted by the ionic interaction, the attachment rates k_{-2} and/or k_4 would decrease with an increase in IS. However, this effect is very small (k_{-2} in Fig. 7b) to none (k_4 in Fig. 10b), demonstrating that the electrostatic force may not contribute to the attachment process. Instead, we found that the detachment rates k_2 and k_{-4} increase significantly with an increase in IS (Figs. 7b, 10b). This can be explained if the detachment is promoted by a mechanical force caused by a rearrangement of macromolecules, which is counteracted by ionic interaction. Because the counteracting ionic interaction decreases with an increase in IS, the detachment rates k_2 and k_{-4} increase as shown by our experiments (Figs. 7b, 10b).

Ligand binding steps

It is interesting to observe that both ADP (K_0) and ATP (K_1) association constants increased with elevated IS (Figs. 7a, 11f), whereas the Pi association constant (K_5) decreased with IS (Fig. 10a). The latter effect on K_5 is expected for the electrostatic interaction: elevated IS weakens electrostatic force. This happens because Pi is negatively charged by $\sim$1.5 at pH 7.0 on the average, whereas the Pi binding site is positively charged (Lobb et al. 1975) and Pi may have the ionic interaction with K185 in P-loop and R245 in switch 1 (Yount et al. 1995); here, the amino acid residue numbers correspond to those of fast twitch chicken skeletal myosin. On the other hand, our observation that the nucleotide association constants (K_0 and K_1) increased when IS was elevated (Figs. 7a, 11f), cannot be expected from the simple electrostatic interaction. It is possible that a complex force that involves hydrophobic interaction (such as adenine ring and W131 in the pocket (Yount et al. 1995)) and/or ionic repulsion plays a role for the ATP and ADP binding processes, and that the binding pocket becomes more stereospecifically matched to the nucleotide with increased IS. The hydrophobic interaction does not depend on IS.

Force/cross-bridge and series elastic elements

The next question is why does force/cross-bridge (T_{56}) decrease at higher IS (Fig. 10c). It has been thought that force is generated by a rotation of the lever arm around the fulcrum (myosin Gly710) next to the converter domain (Asp719–Asp780), which is initiated by switch 2 that is coupled with γ-phosphate (Geeves & Holmes, 1999) after ATP cleavage (Highsmith et al. 2000). Because this coupling involves the ionic interaction (Geeves et al. 2005), it must occur primarily within the ionic atmosphere. The atmosphere shrinks as IS is raised according to Eq. 5 and as indicated by the solid curve in Fig. 14. If the two elements of the coupling are having Brownian motions, and because their coupling is limited within the Debye length, their average coupling distance must be around half of the Debye length, i.e., $\sim$4 Å at 150 mM IS. This motion is amplified by the lever arm to result in the unitary step size of $\sim$110 Å (Geeves & Holmes, 1999). This coupling diminishes as IS is raised. The close correlation between T_{56} and Debye length as IS is changed (Fig. 14) indicates the significance of this mechanism, and explains lower force at higher IS as observed.

Because elementary force development also depends on the stiffness of in-series elements (Wang and Kawai 2013), we have measured rigor stiffness. The fact, that rigor stiffness did not change with a change in IS (Fig. 13, range 150–300 mM) (see also (Iwamoto 2000) in the range of 200 and 520 mM), demonstrates that the decrease of force at higher IS was not caused by a change in the stiffness of in-series elements including cross-bridges, the thick filament, the thin filament, and the Z-disc. This result also demonstrates that the actin-myosin interface is maintained in the range of IS studied. A good reproducibility of the control tension (95 $\pm$ 2 %) before and after 14 intervening activations at 300 mM IS demonstrates that the 300 mM IS solutions did not extract myosin from sarcomeres. The small decrease in tension (5 $\pm$ 2 %) can be attributed to general run down of the fibres with repeated activations. A very high IS solution (such as 730 mM) is known to extract myosin (Hanson and Huxley 1957).

Correlations to earlier observations

A study suggested that the high IS decreases the number of attached cross-bridges in active muscle by increasing the detachment rate, and this increased detachment occurs because the initially attached cross-bridges are moved to other states where they remain attached to generate force (Seow and Ford 1993). This suggestion is generally consistent to ours, although their mechanism is not as detailed as ours. The facts that larger K_1, K_2 (Fig. 7a), and $1/K_5$ (reciprocal of Fig. 10a) in larger IS solutions demonstrate the accelerated ATP binding, and the increased cross-bridge detachment rates (less force). This is helped by smaller K_4 (Fig. 10a) in larger IS. The combined effects result in an inefficient energy usage at higher IS. We reported that elevated IS depressed isometric tension and the

ATP hydrolysis rate, but the effect was much larger on tension than on the hydrolysis rate (Kawai et al. 1990). Sugi et al. (Sugi et al. 2013) found in a recent report that the maximum unloaded shortening velocity (V_{max}) of Ca^{2+}-activated fibres remained unchanged at low IS, despite the increased stiffness of relaxed fibres. The value of stiffness at 0 mM KCl was about four times larger than that at the standard KCl concentration (125 mM); little change in the ATP hydrolysis rate was observed on Ca^{2+}-activated fibres at low IS, when isometric tension increased two-fold (Sugi et al. 2013). They suggested that, at low IS, the force generated by individual myosin heads increases up to two-fold, while the kinetics of the actomyosin interaction coupled with ATP hydrolysis remain unchanged (Sugi et al. 2013). Our results demonstrate that the decrease in force per cross-bridge with IS (Fig. 10c) is the primary mechanism of the IS effect, but also the number of force-generating cross-bridges decreases as the secondary mechanism and as shown in Fig. 12. The cross-bridge kinetics are significantly affected by the IS change as seen its effects on K_0, K_1, k_2, k_{-4}, and K_5.

Other considerations

We found that the higher IS caused a decrease in tension, which is accompanied by a much smaller decrease in stiffness (Fig. 2a, b). A couple of possibilities exist to explain this phenomenon. Firstly, the higher IS causes a transition of the strongly attached cross-bridges to the weakly attached cross-bridges (Fig. 12; AMS and AMDP in Scheme 1), which may correspond to the previous observation that high IS retains the number of cross-bridges in the low force states and thereby decreases isometric tension (Seow and Ford 1993). This is realized by the attached cross-bridges that contribute to stiffness but not to force (Colombini et al. 2010). Our results demonstrate that the number of strongly attached cross-bridges (Fig. 12, Att) decreases similarly to stiffness (Fig. 2a, b) with an increase in IS.

Conclusion

The markedly decreased force per cross-bridge and decreased number of strongly attached cross-bridges at high IS can collectively result in the decreased tension production in muscle fibres, where the decreased force/cross-bridge plays a more significant role than the decreased number of cross-bridges. The effect of IS on muscle contractility is based on cross-bridge kinetics, but not on series elastic elements. An increase in IS affects the cross-bridge kinetics via increases in nucleotide binding steps (K_0, K_1), cross-bridge detachments steps (k_2, k_{-4}), and the phosphate release step ($1/K_5$) in the cross-bridge cycle. The significance of our findings is that the final step of force generation is promoted by the electrostatic interaction: this interaction is diminished at higher IS because the ionic atmosphere shrinks to result in a less power stroke hence less force/cross-bridge; that the electrostatic force between Pi and myosin promotes their binding, whereas the electrostatic force does not promote ATP and ADP binding to myosin.

Acknowledgments This work was supported by grants from the National Institutes of Health HL070041 (MK), and The American Heart Association 13GRNT16810043 (MK). This study was carried out during Dr. Anzel Bahadir's visit to The University of Iowa with a scholarship (82444403-299-1926) funded by Higher Educational Council of Turkey. The content is solely the responsibility of the authors and does not necessarily reflect the official views of the funding organizations.

Conflict of interest The authors have no conflicts of interests.

References

Andrews MA, Maughan DW, Nosek TM, Godt RE (1991) Ion-specific and general ionic effects on contraction of skinned fast-twitch skeletal muscle from the rabbit. J Gen Physiol 98(6):1105–1125

Borejdo J, Szczesna-Cordary D, Muthu P, Calander N (2010) Familial hypertrophic cardiomyopathy can be characterized by a specific pattern of orientation fluctuations of actin molecules. Biochemistry 49(25):5269–5277

Candau R, Kawai M (2011) Correlation between cross-bridge kinetics obtained from Trp fluorescence of myofibril suspensions and mechanical studies of single muscle fibers in rabbit psoas. J Muscle Res Cell Motil 32(4–5):315–326

Colombini B, Nocella M, Bagni MA, Griffiths PJ, Cecchi G (2010) Is the cross-bridge stiffness proportional to tension during muscle fiber activation? Biophys J 98(11):2582–2590

Geeves MA, Fedorov R, Manstein DJ (2005) Molecular mechanism of actomyosin-based motility. Cell Mol Life Sci 62(13):1462–1477

Geeves MA, Holmes KC (1999) Structural mechanism of muscle contraction. Annu Rev Biochem 68:687–728

Godt RE, Maughan DW (1988) On the composition of the cytosol of relaxed skeletal muscle of the frog. Am J Physiol 254(5 Pt 1):C591–C604

Gordon AM, Godt RE, Donaldson SK, Harris CE (1973) Tension in skinned frog muscle fibers in solutions of varying ionic strength and neutral salt composition. J Gen Physiol 62(5):550–574

Gulati J, Podolsky RJ (1978) Contraction transients of skinned muscle fibers: effects of calcium and ionic strength. J Gen Physiol 72(5):701–715

Gulati J, Podolsky RJ (1981) Isotonic contraction of skinned muscle fibers on a slow time base: effects of ionic strength and calcium. J Gen Physiol 78(3):233–257

Hanson J, Huxley HE (1957) Quantitative studies on the structure of cross-striated myofibrils. II. Investigations by biochemical techniques. Biochim Biophys Acta 23(2):250–260

Heinl P, Kuhn HJ, Ruegg JC (1974) Tension responses to quick length changes of glycerinated skeletal muscle fibres from the frog and tortoise. J Physiol 237(2):243–258

Highsmith S, Polosukhina K, Eden D (2000) Myosin motor domain lever arm rotation is coupled to ATP hydrolysis. Biochemistry 39(40):12330–12335

Huxley AF (1974) Muscular contraction. J Physiol 243(1):1–43

Iwamoto H (2000) Influence of ionic strength on the actomyosin reaction steps in contracting skeletal muscle fibers. Biophys J 78(6):3138–3149

Kawai M (1982) Correlation between exponential processes and cross-bridge kinetics. Soc Gen Physiol Ser 37:109–130

Kawai M (1986) The role of orthophosphate in crossbridge kinetics in chemically skinned rabbit psoas fibres as detected with sinusoidal and step length alterations. J Muscle Res Cell Motil 7(5):421–434

Kawai M, Brandt PW (1980) Sinusoidal analysis: a high resolution method for correlating biochemical reactions with physiological processes in activated skeletal muscles of rabbit, frog and crayfish. J Muscle Res Cell Motil 1(3):279–303

Kawai M, Halvorson HR (1989) Role of MgATP and MgADP in the cross-bridge kinetics in chemically skinned rabbit psoas fibers. Study of a fast exponential process (C). Biophys J 55(4):595–603

Kawai M, Halvorson HR (1991) Two step mechanism of phosphate release and the mechanism of force generation in chemically skinned fibers of rabbit psoas muscle. Biophys J 59(2):329–342

Kawai M, Zhao Y (1993) Cross-bridge scheme and force per cross-bridge state in skinned rabbit psoas muscle fibers. Biophys J 65(2):638–651

Kawai M, Wray JS, Guth K (1990) Effect of ionic strength on crossbridge kinetics as studied by sinusoidal analysis, ATP hydrolysis rate and X-ray diffraction techniques in chemically skinned rabbit psoas fibres. J Muscle Res Cell Motil 11(5):392–402

Kawai M, Kido T, Vogel M, Fink RH, Ishiwata S (2006) Temperature change does not affect force between regulated actin filaments and heavy meromyosin in single-molecule experiments. J Physiol 574(Pt 3):877–887

Kerrick WG, Kazmierczak K, Xu Y, Wang Y, Szczesna-Cordary D (2009) Malignant familial hypertrophic cardiomyopathy D166 V mutation in the ventricular myosin regulatory light chain causes profound effects in skinned and intact papillary muscle fibers from transgenic mice. FASEB J 23(3):855–865

Lobb RR, Stokes AM, Hill HA, Riordan JF (1975) Arginine as the C-1 phosphate binding site in rabbit muscle aldolase. FEBS Lett 54(1):70–72

Maughan DW, Godt RE (1980) A quantitative analysis of elastic, entropic, electrostatic, and osmotic forces within relaxed skinned muscle fibers. Biophys Struct Mech 7(1):17–40

Mettikolla P, Calander N, Luchowski R, Gryczynski I, Gryczynski Z, Zhao J, Szczesna-Cordary D, Borejdo J (2011) Cross-bridge kinetics in myofibrils containing familial hypertrophic cardiomyopathy R58Q mutation in the regulatory light chain of myosin. J Theor Biol 284(1):71–81

Moore WJ (1962) Physical Chemistry, 3rd edn. Prentice Hall, Englewood Cliffs

Seow CY, Ford LE (1993) High ionic strength and low pH detain activated skinned rabbit skeletal muscle crossbridges in a low force state. J Gen Physiol 101(4):487–511

Sugi H, Abe T, Kobayashi T, Chaen S, Ohnuki Y, Saeki Y, Sugiura S (2013) Enhancement of force generated by individual myosin heads in skinned rabbit psoas muscle fibers at low ionic strength. PLoS One 8(5):e63658

Thames MD, Teichholz LE, Podolsky RJ (1974) Ionic strength and the contraction kinetics of skinned muscle fibers. J Gen Physiol 63(4):509–530

Wang L, Kawai M (2013) A re-interpretation of the rate of tension redevelopment (k(TR)) in active muscle. J Muscle Res Cell Motil 34(5–6):407–415

Wang Y, Xu Y, Kerrick WG, Wang Y, Guzman G, Diaz-Perez Z, Szczesna-Cordary D (2006) Prolonged Ca^{2+} and force transients in myosin RLC transgenic mouse fibers expressing malignant and benign FHC mutations. J Mol Biol 361(2):286–299

Wang L, Muthu P, Szczesna-Cordary D, Kawai M (2013) Diversity and similarity of motor function and cross-bridge kinetics in papillary muscles of transgenic mice carrying myosin regulatory light chain mutations D166 V and R58Q. J Mol Cell Cardiol 62:153–163

Wang L, Ji X, Sadayappan S, Kawai M (2014) Phosphorylation of cMyBP-C affects contractile mechanisms in a site-specific manner. Biophys J 106(5):1112–1122

Yan Q, Sun Y, Lin J (1996) A quantitative study on the effect of breathing exercises in improving respiratory muscle contration. Zhonghua nei ke za zhi 35(4):235–238

Yount RG, Lawson D, Rayment I (1995) Is myosin a "back door" enzyme? Biophys J 68(4 Suppl):44S–47S; discussion 47S–49S

Zhao Y, Kawai M (1994) Kinetic and thermodynamic studies of the cross-bridge cycle in rabbit psoas muscle fibers. Biophys J 67(4):1655–1668

Zhao Y, Kawai M (1996) Inotropic agent EMD-53998 weakens nucleotide and phosphate binding to cross bridges in porcine myocardium. Am J Physiol 271(4 Pt 2):H1394–H1406